Astron. Astrophys. 349, 406–410 (1999)

ASTRONOMY AND ASTROPHYSICS

ISO far-infrared observations of rich galaxy clusters⋆

I. Abell 2670

L. Hansen[1], H.E. Jørgensen[1], H.U. Nørgaard-Nielsen[2], K. Pedersen[2], P. Goudfrooij[3,⋆⋆], and M.J.D. Linden-Vørnle[1,2]

[1] Copenhagen University Observatory, Juliane Maries Vej 30, DK-2100 Copenhagen, Denmark
[2] Danish Space Research Institute, Juliane Maries Vej 30, DK-2100 Copenhagen, Denmark
[3] Space Telescope Science Institute, 3700 San Martin Drive, Baltimore, MD 21218, USA

Received 7 June 1999 / Accepted 19 July 1999

Abstract. As part of an investigation of far-infrared emission from rich galaxy clusters the central part of Abell 2670 has been mapped with ISO at $60\,\mu$m, $100\,\mu$m, $135\,\mu$m, and $200\,\mu$m using the PHT-C camera. Point sources detected in the field have infrared fluxes comparable to normal spirals at the cluster distance. Probable optical counterparts are cluster galaxies with various characteristics such as blue colour, Hα emission, or double nuclei. One source is extended which could possibly be emission from intracluster dust in debris from spiral galaxies.

Key words: galaxies: clusters: individual: Abell 2670 – infrared: galaxies

1. Introduction

We have observed a sample of five rich galaxy clusters with the Infrared Space Observatory (ISO) satellite, using the PHT-C camera (Lemke et al. 1996) at $60\,\mu$m, $100\,\mu$m, $135\,\mu$m, and $200\,\mu$m. In these clusters cooling flows have been inferred from X-ray observations with mass deposition rates ranging from forty to several hundred $\mathrm{M}_\odot\ \mathrm{yr}^{-1}$ (White et al. 1997). One motivation was to test the hypothesis (Hansen et al. 1995) that most of this mass is transformed into low-mass stars. During the star formation process dust is assumed to be formed, and a significant fraction is returned to the hot gas phase, heated and destroyed by sputtering. The heating of the grains is counter balanced by infrared emission, which can be calculated from the mass deposition rate, the density of optical light, and the density and temperature of the X-ray-emitting gas.

In the present paper we present results for Abell 2670. The cluster (z=0.076, richness class 3, Bautz-Morgan type I-II) is dominated by a central cD galaxy and has recently been shown to consist of several merging subclusters (Bird 1994; Hobbs & Willmore 1997). Cox et al. (1995) used $60\,\mu$m and $100\,\mu$m IRAS ADDSCAN data to search for far-infrared emission in Abell clusters. A signal from Abell 2670 was measured in the $100\,\mu$m band at a 98% confidence level and of a large extent giving a suspicion of Galactic cirrus, but because the source was extended and no significant signal was found at $60\,\mu$m, it was classified as a non-detection according to their adopted criteria. The mass deposition rate in the cooling flow of Abell 2670 is low based on EINSTEIN IPC data ($41\ \mathrm{M}_\odot\ \mathrm{yr}^{-1}$, White et al. 1997). Estimated ISO fluxes from our model (Hansen et al. 1995) within the cooling radius ($\approx 1'$) are given in Table 1.

Table 1. Estimated infrared emission from intracluster dust in Abell 2670 predicted from our hypothesis. The fluxes (in Jy) are calculated assuming a mass deposition rate of $41\ \mathrm{M}_\odot\ \mathrm{yr}^{-1}$ and are expected within the cooling radius ($\approx 1'$)

	$60\,\mu$m	$100\,\mu$m	$135\,\mu$m	$200\,\mu$m
model	0.01	0.02	0.02	0.02

2. Observations

2.1. The ISO data

Abell 2670 was imaged by ISO during revolution 371 (November 21, 1996) in $60\,\mu$m, $100\,\mu$m, $135\,\mu$m, and $200\,\mu$m using the far infrared camera PHT-C. The 9 pixel C100 detector was used for $60\,\mu$m and $100\,\mu$m and the 4 pixel C200 for $135\,\mu$m, and $200\,\mu$m. The observing mode was PHT 32 performing mapping of the sky by moving the telescope in a raster along the spacecraft Y and Z directions. A raster is made for one filter at a time. In the Y direction the chopping mirror allows an overlap in sky coverage between adjacent raster pointings, and a scan along the Y direction is performed. After a step in the Z direction a parallel scan is performed with a certain overlap in sky coverage. With the oversampling factors used in the Z steps the overlaps become $46''$ and $92''$, respectively. The fixed chopper steps in Y are $15''$ for C100 and $30''$ for C200. The resulting images there-

Send offprint requests to: L. Hansen

⋆ Based on observations with ISO, an ESA project with instruments founded by ESA member states (especially the PI countries: France, Germany, the Netherlands, and the United Kingdom) and with the participation of ISAS and NASA

⋆⋆ Affiliated to the Astrophysics Division, Space Science Department, European Space Agency
Correspondence to: leif@astro.ku.dk

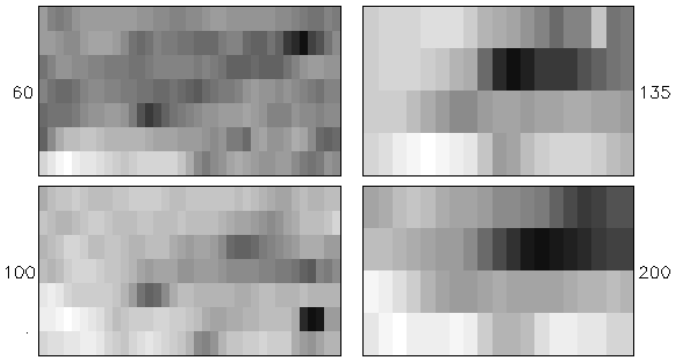

Fig. 1. The brightness images from the PIA reductions. Maximum brightness is dark. Value ranges in $\mathrm{MJy\,sr^{-1}}$ are: 14.7–17.8 ($60\,\mu$m), 9.2–13.6 ($100\,\mu$m), 6.3–8.3 ($135\,\mu$m), 3.6–5.4 ($200\,\mu$m). The field is $9\farcm3 \times 5\farcm4$ for C100 and $9\farcm6 \times 6\farcm2$ for C200. An optical image of the field is shown in Fig. 3

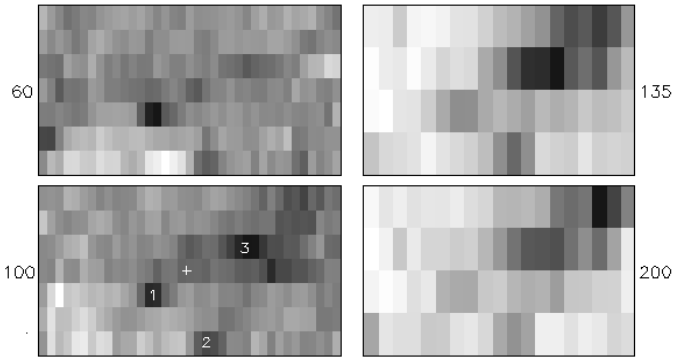

Fig. 2. The LSQ images. The data are the same as displayed in Fig. 1, but reduced by our least squares procedure. In the $100\,\mu$m image the plus marks the center of the cD, and the numbers 1, 2, and 3 mark sources discussed in the text and also labeled in Fig. 3 as S1, S2, and S3

fore have natural pixel sizes of $15'' \times 46''$ and $30'' \times 92''$. In comparison the instrumental resolution measured as the FWHM of the point spread functions available in the ISOPHOT Interactive Analysis software[1] (PIA, version V7.1.1e) are about $50''$ for C100 and $95''$ for C200.

2.2. Reductions

The results presented in Fig. 1 are based on images batch processed by PIA. The flux calibrations are based on both calibration lamps which were observed before and after each scan. Linear interpolation between the two measurements was applied. When the mapping was performed background flat fielding was selected.

We also presents results for the *same* data in Fig. 2 where a least squares reduction procedure (LSQ) has been used. The LSQ procedure was worked out by us at a time when PIA was not sufficiently developed to give useful results for PHT 32 data and is, therefore, independent of PIA. The method rely on the fact, that the flux from the individual sky pixels is measured by various detector pixels at different times making a relative sensitivity calibration of the latter possible. The procedure is simple in the sense that the only further assumptions made are, (1) that the detector voltage increases linearly with time proportional to the incoming flux, and (2) that the dark corrections available in the calibration files belonging to PIA apply. A problem in the data is the numerous glitches present after cosmic ray hits. While PIA uses refined methods to correct for such glitches our procedure simply discards large residuals iteratively. The resulting images (Fig. 2) are in the following denoted LSQ images. Although the results obtained in this way do not make optimum use of the data, we still regard a comparison between the LSQ and PIA images as useful until more experience with such data has been obtained.

[1] The ISOPHOT data presented in this paper was reduced using PIA, which is a joint development by the ESA Astrophysics Division and the ISOPHOT consortium.

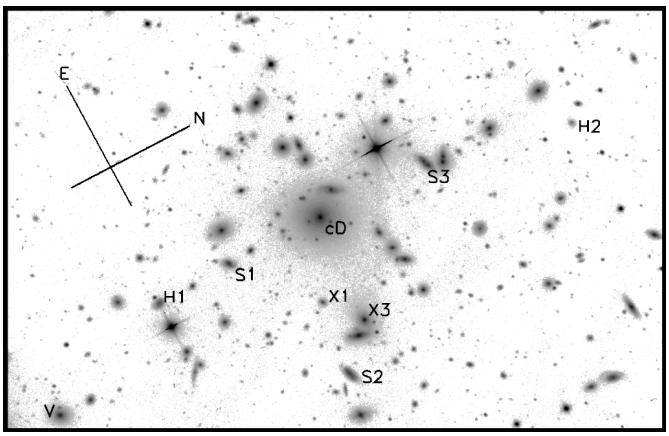

Fig. 3. An optical image of Abell 2670 covering the C200 field of Figs. 1 and 2 ($9\farcm6 \times 6\farcm2$). The cD galaxy is at the center. Possible counterparts to infrared sources are labeled S1, S2, and S3. S3 is a pair of interacting galaxies. Objects H1, H2, S2, and the southern component of the S3 pair are detected sources of Hα emission. X1 and X3 are X-ray sources. Object V is a faint radio source detected with the VLA. The intensity scale is logarithmic

2.3. Optical imaging

Fig. 3 reproduces a stacked optical image of Abell 2670 obtained with the Danish 1.54m telescope at La Silla, Chile, in September 1996. The individual images were exposed through the following filters: B (30 min), V (10 min), and Gunn I (15 min). Fig. 3 covers the C200 field of Figs. 1 and 2 and is centered on the dominant cD galaxy. Notice, that north is towards upper right corner.

Narrow band images were also obtained in the same observing run. One filter (λ7102, FWHM = 80 Å) covered the redshifted Hα+[N II] lines, and the other (λ6960, FWHM = 71 Å) fall in the nearby continuum. After rotation, scaling, and subtraction of these images a Hα+[N II] image resulted. Inspection of the Hα+[N II] image revealed nebular emission in four galaxies within the field of the ISO scan. No emission was found associated with the cD galaxy. The four emission-line galaxies

are marked H1, H2, S2, and S3 in Fig. 3, and further comments are given below.

H1: Identical to galaxy #74 in the list of Sharples et al. 1988. The object is not associated with any of the stronger infrared sources visible in Figs. 1 and 2. The small object just east of the nucleus is probably a star.
H2: Sharples et al. 1988 #281. Not obviously associated with infrared emission.
S2: Galaxy #28 of Sharples et al. 1988. An infrared source is seen at this position in all four bands.
S3: A pair of galaxies. The southern is #7 and the northern #9 of Sharples et al. (1988). Both galaxies have double nuclei. The nebular emission is detected in the eastern component of #7. The galaxies are probably interacting. An infrared source is detected at the position of the pair.

2.4. X-ray and radio sources

Hobbs & Willmore (1997) discovered 3 point-like X-ray sources in the field from ROSAT HRI data. Their sources 1 and 3 coincide with optical objects which are marked X1 and X3 in Fig. 3. Source 2 is situated in between X1 and X3 without an optical counterpart. There are no known quasars in the field (NASA/IPAC Extragalactic Database[2]).

Slee et al. (1996) surveyed rich clusters of galaxies at 1.5 and 4.9 GHz with the VLA. The limit extends to 1 mJy at 1.5 GHz, and 15 sources were detected in the area of Abell 2670. Number 15 was identified with an early type galaxy (Sharples et al. 1988 #40) just visible in the lower left corner of Fig. 3 (object V), i.e. in the C200 field but slightly below the C100 field. The flux of source number 15 at 1.5 GHz is 2.7 mJy with no detection at 4.9 GHz. Hacking et al. (1989) made 1.49 GHz VLA maps of $60\,\mu\mathrm{m}$ sources detected in a deep IRAS survey. They find a typical infrared to radio flux of about 100, and we therefore expect a $60\,\mu\mathrm{m}$ flux of 200–300 mJy. We made the experiment to put an infrared source of this strength at the position of object V, but found that too little flux is scattered into our $60\,\mu\mathrm{m}$ frame to be detectable.

3. Results

When Figs. 1 and 2 are compared some noticeable similarities and differences are seen. The $60\,\mu\mathrm{m}$ PIA image has a strong feature in the upper right corner which is not visible in the LSQ image, nor in the other pass-bands. Similarly the $100\,\mu\mathrm{m}$ PIA image has two strong features near the right border which are not present in any other image. These are probably artefacts. On the other hand the three features marked 1, 2, and 3 in Fig. 2 appear persistently in both reductions and in at least three pass-band. We regard these as real sources. Their reality was also confirmed by a procedure used by Linden-Vørnle et al. (1999). They use a median filtering technique, where the PIA reduced data are corrected for drift effects before mapping in order to enhance the detection of point sources.

The three infrared sources fall within $10''$ from galaxies marked S1, S2, and S3 in Fig. 3. As shown by the following remarks these objects have signs of enhanced star formation activity.

S1: The galaxy is #86 in the list of Sharples et al. 1988. It has been classified as S0, but has a blue colour indicative of recent star formation (Table 3).
S2: Sharples et al. 1988 #28. This is one of our detected sources of nebular emission which can be explained by star formation activity.
S3: A pair of galaxies (#7 and #9 of Sharples et al. 1988) both of which show double nuclei. Their radial velocities differ by $420\,\mathrm{km\,s^{-1}}$ (Sharples et al. 1988). The overlapping optical isophotes, the presence of double nuclei, and the detected nebular emission in #7 point to galaxy encounters with associated star formation activity.

Because star formation is known to be associated with infrared emission from warm dust, it is reasonable to assume that the three optical objects are the counterparts of the infrared sources.

There are further infrared features in Figs. 1 and 2 which may be real, such as a possible source marked with a plus sign in Fig. 2 associated with the cD galaxy. Particularly at longer wavelengths the features form a diagonal band from the upper right towards the lower left thus following the chain of cluster galaxies oriented north-south through the cluster center. In Fig. 4 the $100\,\mu\mathrm{m}$ PIA image is reproduced overlaid with a contour plot of Fig. 3. The tendency for the infrared emission to follow the optical contours favours the interpretation, that the emission is associated with the cluster.

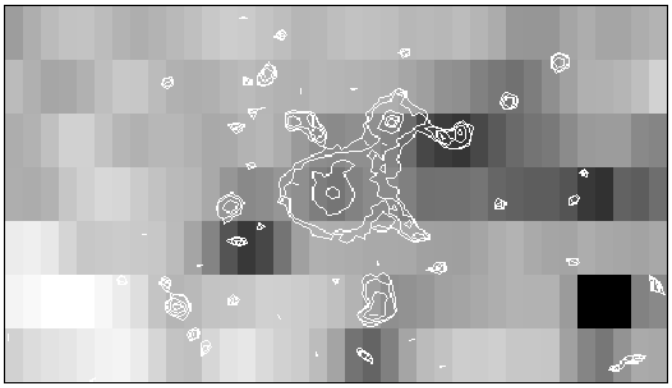

Fig. 4. A contour map of the optical image (Fig. 3) is overlaid the $100\,\mu\mathrm{m}$ PIA image. The infrared emission has a tendency to follow the distribution of galaxies. Two apparent infrared sources near the right edge are artefacts

3.1. Flux measurements

A procedure has been developed to do aperture photometry on sources in the PIA brightness images. We use circular apertures and interpolate the included area for pixels on the rim. Aperture

[2] The NASA/IPAC Extragalactic Database (NED) is operated by the Jet Propulsion Laboratory, California Institute of Technology, under contract with the National Aeronautics and Space Administration

Table 2. Aperture photometry on objects with model predicted fluxes

object	filter	model flux	measured	deviation
HR 5981	$60\,\mu$m	0.142	0.15	+06
IRC+60228	$90\,\mu$m	0.084	0.07	-17
HR 1654	$135\,\mu$m	0.254	0.25	-02
HR 1654	$160\,\mu$m	0.197	0.30	+52
		Jy	Jy	%

corrections are calculated based on the point spread functions used in PIA.

The procedure can be checked by means of observed standard stars for which accurate model predictions are available[3]. The sources were observed in raster scans (PHT32) like Abell 2670. The FIR calibrations for the standard stars were obtained by fitting the shape of an appropriate red giant branch star model to the longest wavelength observations reliably measured for these stars, thus extending the SEDs out to $300\,\mu$m (Cohen et al. 1996, Cohen private communication). The results of our aperture photometry are compared with the model predictions in Table 2. The deviations are compatible with the present ISOPHOT calibration accuracies of 20% (Klaas et al. 1998), although the deviation is rather large for the $160\,\mu$m measurement.

In our procedure the flux measured in the aperture is corrected for the background level, which is usually the dominant error source. We derive the background value from the median brightness of the image. The $160\,\mu$m image of HR 1654 shows significant structure in the background. However, in such cases – which also apply to our Abell 2670 frames – a better procedure is to position, scale, and subtract the PSF from the image. If this is performed for the HR 1654 $160\,\mu$m image using the flux value given in Table 2 an obvious over-correction is seen. When we lower the assumed flux until the background looks smooth the flux is reduced from 0.30 to 0.21 Jy, which is only a 7% deviation from the model flux. In what follows we therefore use the PSF subtraction method.

3.2. ISO sources

We have identified 3 certain sources (S1, S2, and S3) in the ISO images (Figs. 1 and 2). By varying the flux and subtracting the PSF an upper and a lower flux limit can be estimated (cf. 3.1). From these limits the mean and its deviation from the limits have been calculated and are given in Table 3. A possible signal at the position of the cD may be present in the $100\,\mu$m image and has been measured. For $60\,\mu$m only an upper limit can be given for the cD, and for $135\,\mu$m and $200\,\mu$m source confusion prevents a reliable estimate.

Some comments on S3 are necessary. S3 appears in an area of enhanced background emission. The source is ill defined in the $60\,\mu$m PIA image, but is somewhat more convincing in the LSQ image. At $100\,\mu$m both reduction methods agree about the source. At $135\,\mu$m and $200\,\mu$m the source becomes the brightest in the area, but broader than compatible with a single point source. In the $135\,\mu$m PIA image the peak is shifted two pixels to the left, but this is likely an artefact and not seen in the LSQ image. At $200\,\mu$m S3 peaks at the position of the optical pair.

[3] These data were kindly put to our disposal by Ulrik Klaas, ISOPHOT Data Centre

4. Discussion

The tendency of the infrared emission to follow the distribution of galaxies makes it likely that it is associated with the cluster rather than being foreground cirrus. The reality of sources S1, S2, and S3 is well established. S1 and S2 are probably associated with cluster galaxies with star formation activity. S3 is identified as a pair of apparently interacting galaxies, both with a double nucleus. The southern component shows nebular emission. One or more galaxy encounters with triggered star formation and associated infrared emission is therefore very likely. Melnick & Mirabel (1990) studied *ultraluminous* infrared galaxies and found all to be advanced mergers with double nuclei and tails. They suggest that a critical distance of about 10 kpc is required for the system to become ultraluminous. In #7 the distance between the nuclei is 7.2 kpc, and in #9 it is 6.7 kpc (for $\mathrm{H}_\circ = 75\,\mathrm{km\,s^{-1}\,Mpc^{-1}}$ as used by Melnick & Mirabel 1990). The distance between the nearest nuclei in the galaxy pair is 19.6 kpc. The sources in Abell 2670 are, however, not particularly strong compared to normal field galaxies. Alton et al. (1998) have published infrared data for 7 nearby spiral galaxies representing quiescent galaxies with normal FIR-to-blue colours. IRAS (HiRes) fluxes are given for $60\,\mu$m and $100\,\mu$m together with ISOPHOT fluxes for $200\,\mu$m. In Table 3 we present data for these objects scaled to the distance of Abell 2670. The properties of S1, S2, and S3 are quite compatible with this sample.

S3 is extended at $135\,\mu$m and $200\,\mu$m. The reason could be an instrumental artefact or galactic foreground emission accidentally projected on the cluster galaxies. However, the spatial coincidence with a pair of interacting galaxies favours the interpretation that we are detecting intergalactic dust in the cluster – possibly related to galaxy debris either from galaxy encounters forming the S3 pair, or due to ram pressure stripping working on galaxies moving through the intracluster gas. As mentioned in the introduction, Abell 2670 consists of several merging subclusters and is thus in a highly active dynamical state.

As stated in Sect. 1 a goal of the present study is to search for a possible dust component of the hot intracluster gas. The predicted fluxes are at a level of 0.01–0.02 Jy for Abell 2670 (Table 1) within the cooling radius ($\approx 1'$). The X-ray emission peaks at the cD (Hobbs & Willmore 1997), and we therefore expect the hypothetical infrared emission to occur more or less within the visible envelope of the cD. The data presented for the cD in Table 3 do not rule out the model, but do not pose any strong constraints either. At the long wavelengths source confusion prevents a study of the predicted effect. Even if point source subtraction could be accurately made, the extended nature of S3 covering part of the cooling area masks the hypothetical, faint

Table 3. Source fluxes determined from the PIA images (Jy) by positioning, scaling, and subtracting the PSF. The quoted uncertainties are *not* statistical, but are subjectively evaluated limits as described in the text. B, B-V, and T (morphology parameter of de Vaucouleurs et al. 1976) are from Sharples et al. (1988). Also given are observed data for nearby spirals (Alton et al. 1998) scaled to the distance of Abell 2670. K-corrections for optical data are taken from Pence (1976)

Object	$60\,\mu$m	$100\,\mu$m	$135\,\mu$m	$200\,\mu$m	B	B-V	T	comments
cD	< 0.03	0.09 ± 0.05	–	–	15.7	1.18	-4	
S1	0.11 ± 0.03	0.19 ± 0.04	0.13 ± 0.09	0.15 ± 0.08	18.5	0.94	-2	blue colour
S2	0.06 ± 0.03	0.14 ± 0.04	0.25 ± 0.10	0.17 ± 0.08	17.7	0.92	9	Hα emission
S3	0.04 ± 0.02	0.13 ± 0.05	0.28 ± 0.15	0.45 ± 0.25	17.2	1.12	0	interacting pair
NGC 134	0.11	0.33		0.63	17.2	1.00	4	
NGC 628	0.02	0.06		0.18	17.8	0.72	5	
NGC 660	0.10	0.17		0.22	19.4	1.01	1	
NGC 5194	0.06	0.13		0.23	17.6	0.76	4	
NGC 5236	0.17	0.33		0.47	16.5	0.81	5	
NGC 6946	0.19	0.38		0.84	17.1	0.96	6	
NGC 7331	0.06	0.16		0.32	17.9	1.04	4	

extended flux. The upper limit measured at $60\,\mu$m and the point source flux measured at $100\,\mu$m at the position of the cD already exceeds the model predictions. We therefore conclude that the data for Abell 2670 does not allow us to perform a convincing test of our hypothesis due to the presence of point sources and extended emission possibly related to the ongoing merging of subclusters in Abell 2670. In forthcoming papers other rich clusters will be studied and compared to Abell 2670.

Acknowledgements. This work has been supported by The Danish Board for Astronomical Research.

References

Alton P.B., Trewhella M., Davies J.I., et al., 1998, A&A 335, 807
Bird C., 1994, ApJ 422, 480
Cohen M., Witteborn F.C., Carbon D.F., Wooden D.H., Bregman J.D., 1996, AJ 112, 2274
Cox C.V., Bregman J.N., Schombert J.M., 1995, ApJS 99, 405
de Vaucouleurs G., de Vaucouleurs A., Corwin H.G., 1976, Second Reference Catalogue of Bright Galaxies. University of Texas Press, Austin
Hacking P., Condon J.J., Houck J.R., Beichman C.A., 1989, ApJ 339, 12
Hansen L., Jørgensen H.E., Nørgaard-Nielsen H.U., 1995, A&A 297, 13
Hobbs I.S., Willmore A.P., 1997, MNRAS 289, 685
Klaas U., Laureijs R.J., Radovich M., Schulz B., 1998, ISOPHOT Calibration Accuracies. ISOPHOT technical report SAI/98-092/Dc
Lemke D., Klaas U., Abolins J., et al., 1996, A&A 315, L64
Linden-Vørnle M.J.D., Nørgaard-Nielsen H.U., Jørgensen H.E., et al., 1999, in preparation for A&A
Melnick J., Mirabel I.F., 1990, A&A 231, L19
Sharples R.M., Ellis R.S., Gray P.M., 1988, MNRAS 231, 479
Pence W., 1976, ApJ 203, 39
Slee O.B., Roy A.L., Andernach H., 1996, Australian J. Phys. 49, 977
White D.A., Jones C., Forman W., 1997, MNRAS 292, 419